Power spectrum and detrended fluctuation analysis: Application to daily temperatures

Peter Talkner and Rudolf O. Weber
General Energy Research, Paul Scherrer Institute, CH-5232 Villigen, Switzerland
(Received 13 January 2000; revised manuscript received 21 March 2000)

The variability measures of fluctuation analysis (FA) and detrended fluctuation analysis (DFA) are expressed in terms of the power spectral density and of the autocovariance of a given process. The diagnostic potential of these methods is tested on several model power spectral densities. In particular we find that both FA and DFA reveal an algebraic singularity of the power spectral density at small frequencies corresponding to an algebraic decay of the autocovariance. A scaling behavior of the power spectral density in an intermediate frequency regime is better reflected by DFA than by FA. We apply FA and DFA to ambient temperature data from the 20th century with the primary goal to resolve the controversy in literature whether the low frequency behavior of the corresponding power spectral densities are better described by a power law or a stretched exponential. As a third possible model we suggest a Weibull distribution. However, it turns out that neither FA nor DFA can reliably distinguish between the proposed models.

PACS number(s): 02.50.Wp, 05.40.−a, 05.45.Tp, 92.60.Ry

I. INTRODUCTION

Time series emerging from complex systems are typically governed by an interplay of random and deterministic mechanisms. The characteristic times of such systems may vary over a large range. As a consequence one often observes a nonexponential decay of correlations of which stretched exponential and algebraic decay are two examples. A precise classification of the decay of correlations is of major importance for the analysis of various natural, technical, and economic systems. The direct estimate of the correlation function of a time series is known to be limited to rather small time lags, and also the determination of the power spectrum is hampered by large statistical uncertainties if one goes to those low frequencies that reflect the long time behavior of the system.

More recently, methods have been suggested to cope with this problem [1–3], and to reliably gain insight into the correlation structure of a time series. These methods are based on the idea of building a running sum over a given time scale. This corresponds to the construction of a random walk that has the values of the original time series as increments. Different quantities characterizing random walks constructed in this way have been suggested to describe the variability of the original time series. In the so-called fluctuation analysis (FA) [1] the average spreads of the random walk during time intervals of lengths s are used to define a variability $F_{FA}(s)$. In the detrended fluctuation analysis (DFA) [3] the mean square deviation from an optimal linear approximation of the random walk during time intervals of length s is introduced as a measure of variability $F_{DFA}(s)$. Further measures have been defined using different wavelet transforms of the random walk [4]. In all these methods one searches for a power law describing the particular fluctuation measure as a function of the scale variable s from which one infers a scaling behavior of the power spectral density, and the covariance function of the original time series.

First applications of FA and DFA were made in investigations of DNA sequences [1–3,5]. Other topics to which FA and DFA were applied are cardiac rhythm fluctuations [6,7] and financial data [8]. Recently, these methods have been used to study meteorological data [4,9–12]. In Ref. [9] daily noon temperatures of several meteorological stations were analyzed by means of DFA. The resulting scaling of the variability implies that the correlation decays as a power law, $\sim t^{-\alpha}$ with exponent $\alpha = 0.7$. This exponent of about 2/3 was also confirmed to characterize daily maximum temperatures in a range of times between ten days and at least 25 years [4,10]. In Ref. [11] a monthly global mean temperature series was analyzed with DFA. Before DFA was applied the data were preprocessed by means of a singular value decomposition in order to remove a possible nonlinear trend. Since this kind of filtering does not act on a predetermined range of frequencies it might also modify the low frequency behavior. It is therefore not clear to what extent the scaling exponent of 0.4 in Ref. [11] is influenced by the data processing.

A main goal of the present paper is to give the general relationships between the different measures of variability $F_{FA}(s)$, $F_{DFA}(s)$ and both the power spectral density and the autocovariance of the underlying process. This allows us to identify corresponding features in the FA and DFA measures of variability, the power spectral density and the correlation function.

In an application of the various methods to daily meteorological data we will show to what extent fluctuation analysis can complement the classical power spectral analysis.

II. METHODS

A. Power spectrum analysis

For a time series $x_i = x(i\Delta t)$, $i = 1, \ldots, N$, which is sampled from a stationary signal $x(t)$ at equidistant times $t = i\Delta t$, the power spectral density $S(\omega)$ can be calculated by a standard nonparametric technique. The time series is divided into K equally long segments overlapping by one-half of their length M. For each segment the periodogram is obtained by applying a Welch window and using a fast Fourier transform [13]. The periodograms of all segments are averaged, reducing the error of the spectral estimate by a factor of about $9K/11$.

 ©2000 The American Physical Society

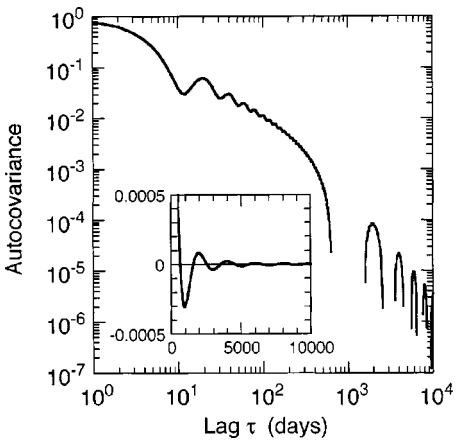

FIG. 1. Autocovariance $C(\tau)$ of a stationary process with a piecewise algebraic power spectral density $S(\omega)=1$ for $\omega<\omega_0$, $S(\omega)=(\omega/\omega_0)^{-0.25}$ for $\omega_0\leqslant\omega<\omega_1$ and $S(\omega)=(\omega_0/\omega_1)^{0.25}(\omega/\omega_1)^{-2}$ for $\omega\geqslant\omega_1$ as a function of frequency. The middle frequency range extends over two orders of magnitude from $\omega_0=2\pi/2000$ to $\omega_1=2\pi/20$. Scales on both axes are logarithmic. There are empty gaps where $C(\tau)$ is negative. No scaling behavior is apparent in the middle range of $20<\tau<2000$. The inset shows the $C(\tau)$ in a linear plot.

The power spectral density $S(\omega)$ is the Fourier transform of the autocovariance $C(\tau)=\langle[x(t+\tau)-\langle x\rangle][x(t)-\langle x\rangle]\rangle$ of the signal,

$$C(\tau)=\frac{1}{2\pi}\int_0^\infty d\omega S(\omega)\cos(\omega\tau). \tag{2.1}$$

Here τ is a time lag and the angular brackets denote the stationary ensemble average. The normalization of the power spectral density is chosen such that the total power is contained in the positive frequencies. If the autocovariance shows a scaling behavior for times larger than τ_1 one also finds a scaling behavior of the power spectrum in the corresponding frequency region $\omega<2\pi/\tau_1$, and vice versa, i.e.,

$$C(\tau)\sim\tau^{-\alpha}\Leftrightarrow S(\omega)\sim\omega^{-\beta}. \tag{2.2}$$

For a stationary time series the autocovariance at time lag $\tau=0$ is finite and consequently the integral of the power spectral density over all frequencies, i.e., the total power also is finite. This restricts the small frequency exponent to $0<\beta<1$. If the long time exponent also takes a value $0<\alpha<1$ the two exponents are related to each other by $\beta=1-\alpha$. For autocovariances decaying faster than t^{-1} the power spectral density approaches a constant value in the limit $\omega\to0$, i.e., $\beta=0$. A possible scaling of the power spectral density, $S(\omega)\sim\omega^{-\beta}$ at large frequencies is restricted to positive scaling exponents β by stationarity.

A scaling regime on a finite interval of frequencies can in principle be identified by means of the scaling of the power spectral density, while the autocovariance does in most cases not show the corresponding algebraic behavior because it is generally obscured by a band of low frequency oscillations, see Fig. 1. Moreover, for large time lags the autocovariance becomes small and at the same time the statistical errors increase. Hence, the feature one is most interested in literally disappears in the noise. The basic idea both of FA and of DFA is to transform the decaying autocovariance into an increasing variability measure, which is less prone to statistical errors.

B. Fluctuation and detrended fluctuation analysis

Fluctuation and detrended fluctuation analysis are recent methods [1,3] used to detect possible long-range correlations in time series. Five variants of fluctuation analysis are described in Ref. [10]. In all variants, in a first step, a running sum of the observed variable x_i, $i=1,\ldots,N$, is calculated

$$y(n)=\sum_{i=1}^{n}x_i, \tag{2.3}$$

where $n=1,\ldots,N$. This sum has been called a landscape [9] or profile [10] of the variable x and it can be viewed as a random walk with increments x_i. We next discuss various variability measures that are based on the so defined random walk.

(i) In fluctuation analysis (FA), this random walk is divided into nonoverlapping segments of length s. The differences of the random walk's positions at the endpoints of the segments

$$\Delta y_k(s)=y(k(s+1))-y((k-1)(s+1)+1) \tag{2.4}$$

are computed for $k=1,\ldots[N/(s+1)]$, where $[x]$ denotes the largest integer smaller than x. The variability $F_{FA}(s)$ over the time scale s is determined as a root mean square difference

$$F_{FA}^2(s)=\left[\frac{N}{s+1}\right]^{-1}\sum_{k=0}^{[N/(s+1)]-1}\Delta y_k(s)^2\equiv\overline{\Delta y(s)^2}, \tag{2.5}$$

where the bar denotes the average over all segments [4]. In the limit $N\to\infty$ for a stationary ergodic process $x(t)$, the time average converges to the ensemble average of the second moment of the increment of the random walk over a segment of length s:

$$F_{FA}^2(s)=\langle\Delta y(s)^2\rangle. \tag{2.6}$$

In Ref. [1] the centered second moment of the differences $\Delta y(s)$ is used. This corresponds to a small constant shift of the variability which has minor influence on a possible scaling.

(ii) In detrended fluctuation analysis (DFA) [3], the linear regressions $\tilde{y}_{k,s}(n)=m_k n+b_k$ of the random walk are performed on all segments k of length s and are subtracted from the random walk on the corresponding segment. The slope m_k and the intercept b_k follow from minimizing the mean square deviation between $y(n)$ and $\tilde{y}_k(n)$ on the segment k. The detrended variability $F_{DFA}(s)$ is defined as the minimum deviation averaged over all segments:

$$F_{DFA}^2(s)=\frac{1}{s+1}\overline{\sum_{n=(k-1)(s+1)+1}^{k(s+1)}[y(n)-\tilde{y}_k(n)]^2}$$
$$=\frac{1}{s+1}\sum_{n=1}^{s+1}\langle[y(n)-\tilde{y}_1(n)]^2\rangle, \tag{2.7}$$

where the bar denotes the average over the segments, and where in the second line, ergodicity of $x(t)$ is assumed. This quantity measures the variability of the original signal at scales that are smaller than the segment length s.

(iii) In Ref. [4] three further methods based on wavelet transforms are suggested for the characterization of the variability. For the data investigated in Ref. [4] all methods yield very similar variabilities up to overall factors. We applied the wavelet methods to ambient temperature data and also found them to yield qualitatively the same results as the simple FA and DFA methods. Therefore, we will only discuss FA and DFA in the following.

III. COMPARISON OF FLUCTUATION ANALYSIS AND POWER SPECTRUM

Both variability measures $F_{FA}(s)$ and $F_{DFA}(s)$ can be related to the power spectral density, or, equivalently, to the autocovariance of the considered time series. Several model power spectral densities, which show the relevant features of the observed temperature spectra as described in Sec. IV below, will be used to determine and discuss the corresponding variability measures. To simplify the resulting equations, a continuously sampled time series is considered in the following. Corrections due to discreteness are shown to be of relevance only for segments that are shorter than approximately 20 sampling times. Corresponding results are given in Appendix A.

A. Fluctuation analysis

For the sake of simplicity we assume that the stationary time series $x(t)$ has zero mean $\langle x(t)\rangle = 0$. The random walk with $x(t)dt$ as infinitesimal increment is given by

$$y(t) = \int_0^t dt' x(t'). \tag{3.1}$$

Accordingly, the distance covered by the random walk on a segment of length s becomes:

$$\Delta y_{s_0}(s) = y(s_0+s) - y(s_0) = \int_{s_0}^{s_0+s} dt x(t), \tag{3.2}$$

and the mean value of the squared variability (2.5) can be written as

$$F_{FA}^2(s) = \langle \Delta y_{s_0}^2(s)\rangle = 2\int_0^s d\tau (s-\tau) C(\tau). \tag{3.3}$$

Expressing the autocovariance in terms of the power spectral density, see Eq. (2.1), one finds:

$$F_{FA}^2(s) = \frac{s}{\pi}\int_0^\infty dw S\left(\frac{w}{s}\right) r_{FA}(w), \tag{3.4}$$

where

$$r_{FA}(w) = \frac{1-\cos(w)}{w^2} \tag{3.5}$$

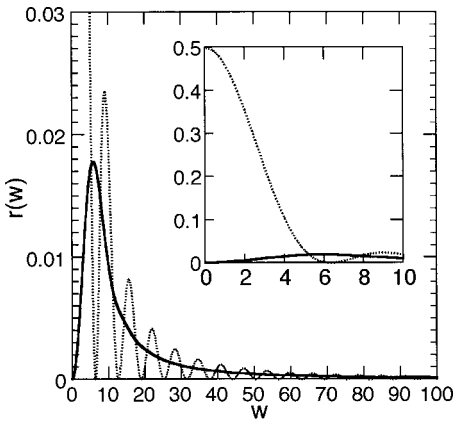

FIG. 2. The frequency filters $r_{FA}(w)$ and $r_{DFA}(w)$ for FA (dotted line) and for DFA (full line), respectively, given by Eqs. (3.5), (3.13), respectively. The inset shows the same functions for small values of the dimensionless frequency w.

acts as a filter on the power spectral density on a logarithmic frequency scale. The filter function $r_{FA}(w)$ is shown in Fig. 2. For white noise, i.e., $C(t-t') = \sigma^2\delta(t-t')$, the squared variability increases linearly in s:

$$F_{FA}^2(s) = \sigma^2 s. \tag{3.6}$$

For an algebraically decaying autocovariance $C(\tau)\sim\tau^{-\alpha}$, $\tau > t_0 > 0$, one finds a variability measure that asymptotically increases with a power law: $F_{FA}^2(s)\sim s^{2-\alpha}$ for $0<\alpha<1$ and $F_{FA}^2(s)\sim s$ for $\alpha>1$. A power spectral density with an algebraic behavior at low frequencies, $S(\omega)\sim\omega^{-\beta}$, also leads to a power law $F_{FA}^2(s)\sim s^{\beta+1}$, in accordance with the relation $\beta = 1-\alpha$ for the scaling exponents with $0<\alpha,\ \beta<1$. The fluctuation measure $F_{FA}^2(s)$ is rather insensitive to the high frequency behavior of the power spectral density and does not resolve different power laws in the high frequency regime. Moreover, if the lag s becomes too short, the discreteness of the time series leads to an increase of the variability compared to the continuum approximation; see also the discussion of finite sampling time effects in Sec. III B. Finally we note that the variability measure based on fluctuation analysis does not properly resolve an intermediate scaling regime of the power spectral density extending over, say, two orders of magnitude in frequency, see Fig. 3.

B. Detrended fluctuation analysis

In detrended fluctuation analysis the linear regression $\tilde{y}_{s_0,s}(t) = m(s_0,s)t + b_k(s_0,s),\ t\in[s_0,s_0+s]$ is calculated by a least-square fit for each segment of length s. The expectation value of the squared variability (2.7) can be written as

$$F_{DFA}^2(s) = \frac{1}{s}\int_{s_0}^{s_0+s} dt_1 \int_{s_0}^{s_0+s} dt_2 \langle y(t_1)y(t_2)\rangle K_{s_0,s}(t_1,t_2), \tag{3.7}$$

where the kernel is defined by

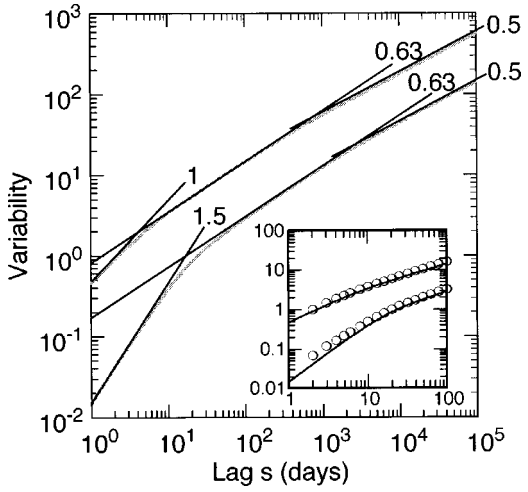

FIG. 3. Variability measures $F_{FA}(s)$ (upper gray curve) and $F_{DFA}(s)$ (lower gray curve) for a piecewise algebraic power spectral density $S(\omega)$ as defined in the caption of Fig. 1. The middle frequency range showing scaling of the power spectral density can be well retrieved as an intermediate scaling regime of $F_{DFA}(s)$ for lags approximately ranging between $s=30$ and $s=1500$. The estimated scaling exponent 0.63 agrees well with its theoretical value $(1+0.25)/2=0.625$. For lags larger than $s\approx 6000$ the detrended fluctuation variability scales with an exponent of 0.5 properly reflecting the constant power spectral density at low frequencies. The increase of $F_{FA}(s)$ with a power 1.5 at small lags is also in quantitative agreement with the high frequency behavior of the spectrum. The variability $F_{DFA}(s)$ scales with an exponent 0.5 for large lags down to $s\approx 1000$ and then turns over into a scaling behavior with exponent 0.63 and falls off below $s=7$ in a steeper way. Hence, FA does not reflect the behavior of the power spectral density in a simple, direct way. Black solid lines refer to exact scaling laws with the indicated exponents. The results for discrete time are shown in the inset as open circles together with the continuous time results (solid lines). Again the upper curve refers to FA and the lower one to DFA.

$$K_{s_0,s}(t_1,t_2)=\delta(t_1-t_2)-\frac{12}{s^3}\left[t_1t_2-\left(s_0+\frac{s}{2}\right)(t_1+t_2)+\left(s_0^2+s_0s+\frac{s^2}{3}\right)\right]. \tag{3.8}$$

It is symmetric in t_1 and t_2, and is stationary and scales in the following sense:

$$K_{s_0,s}(t_1+s_0,t_2+s_0)=K_{0,s}(t_1,t_2)=\frac{1}{s}K_{0,1}\left(\frac{t_1}{s},\frac{t_2}{s}\right). \tag{3.9}$$

Inserting (3.1) and assuming stationarity of the signal $x(t)$, the variability becomes independent of s_0. It is given in terms of the autocovariance $C(\tau)$ by

$$F_{DFA}^2(s)=s^2\int_0^1 du\,C(su)q(u), \tag{3.10}$$

with

$$q(u)=2\int_0^{1-u}dy\int_0^{u-y}dt_1\int_0^y dt_2K_{0,1}(t_1,t_2)=\frac{2}{15}-u+2u^2-\frac{4}{3}u^3+\frac{1}{5}u^5 \tag{3.11}$$

and in terms of the power spectral density $S(\omega)$ by

$$F_{DFA}^2(s)=\frac{s}{2\pi}\int_0^\infty dwS\left(\frac{w}{s}\right)r_{DFA}(w), \tag{3.12}$$

where

$$r_{DFA}(w)=\int_0^1 du\cos(uw)q(u). \tag{3.13}$$

Using the explicit form of $q(u)$ (3.11) we find:

$$r_{DFA}(w)=[w^4-8w^2-24-4w^2\cos(w)+24\cos(w)+24w\sin(w)]w^{-6}. \tag{3.14}$$

Figure 2 compares the filter functions of FA and DFA. Both are positive functions. The most apparent difference between $r_{FA}(w)$ and $r_{DFA}(w)$ are the oscillations in $r_{FA}(w)$ while $r_{DFA}(w)$ consists of a single hump. More important is the fact that $r_{FA}(w)$ has a maximum at $w=0$ whereas $r_{DFA}(s)$ vanishes there. As for the fluctuation analysis the squared detrended variability measure increases linearly with s for white noise. A power spectral density that diverges algebraically as ω vanishes, $S(\omega)\sim\omega^{-\beta}$, results in a scaling behavior of $F_{DFA}^2(s)\sim s^{1+\beta}$ for large s. In this respect we find the same result as from fluctuation analysis. If the power spectral density algebraically decays at large frequencies, $S(\omega)\sim\omega^{-\beta}$, the detrended variability measure increases at small values of s according to the power law $F_{DFA}^2(s)\sim s^{1+\beta}$, provided that $\beta<3$. A power spectral density that decays faster than $S(\omega)\sim\omega^{-3}$ yields $F_{DFA}^2(s)\sim s^4$ for small values of s. This result only holds in the continuum limit. If s becomes smaller than approximately the 20-fold sampling time, the continuum approximation gives too small results. In the inset of Fig. 3 the exact result of the discrete theory, which is sketched in Appendix A, is compared with the continuum approximation (3.12).

In contrast to the variability measure of fluctuation analysis the detrended variability $F_{DFA}(s)$ does reflect an intermediate scaling of the power spectral density and allows one to retrieve the corresponding scaling exponent where

$$F_{DFA}^2(s)\sim s^{1+\beta}\quad\text{for}\quad s_1<s<s_2\quad\Leftrightarrow S(\omega)\sim\omega^{-\beta}\quad\text{for}\quad\frac{2\pi}{s_2}<\omega<\frac{2\pi}{s_1}. \tag{3.15}$$

For an example, see Fig. 3. The frequency range $[2\pi/s_2,2\pi/s_1]$ has to extend over at least two orders of magnitude in order that an intermediate scaling regime is well defined.

C. Finite size effects

From the practical point of view it is important to know to which extent the finiteness of data influences the results of FA and DFA. These finite size effects have been neglected in Eqs. (2.5), (2.7) by assuming that for a given lag s the weighted sum over the corresponding segments does always coincide with the time average over these segments, i.e., that the time average over the segments converges sufficiently fast. This assumption amounts to the self-averaging of the fluctuation measures $F^2_{FA}(s)$ and $F^2_{DFA}(s)$. It is certainly justified for scales $s \ll N$ but becomes questionable if the considered lag approaches the total length of the signal.

Analytic results for the N dependence of the fluctuation measures are difficult to obtain. We therefore performed numerical simulations of time series with given power spectral densities and compared the resulting fluctuation measures with the $N \to \infty$ limit as given by Eqs. (3.4), (3.5), and (3.12), (3.14). As power spectral densities $S(\omega)$ we chose a piecewise power law model, a Weibull distribution and a stretched exponential, which will be shown below to equally well describe the daily ambient temperatures. Using the Wiener-Khinchin theorem, we first construct a series of $N/2=2^k$ frequency-dependent amplitudes $|S(\omega_l)|e^{i\varphi_l}$, $l=1,\ldots,N/2$, with independent random phases φ_l. Upon a fast Fourier transform one obtains a stationary time series of length N having the prescribed power spectral density. Figure 4 shows the results for the DFA measure for synthetic data series of different lengths and different spectral densities. For $N=2^{15}$, comparable with the lengths of the temperature series, up to even the largest scales $s \approx N/3$, the fluctuation measure of the synthetic time series shows only small random deviations from the theoretical result for an infinite series. As one expects, the finite size deviations become smaller for smaller scales s. For a 16 times longer time series finite size effects are almost invisible for all $s \leqslant 10^4$. Accordingly the scatter is increased for $N=2^{11}$ but still allows one to identify a linear scaling regime in the case of the piecewise linear power spectral model. Concerning the finite size effects, the fluctuation analysis behaves very similarly and is therefore not shown here.

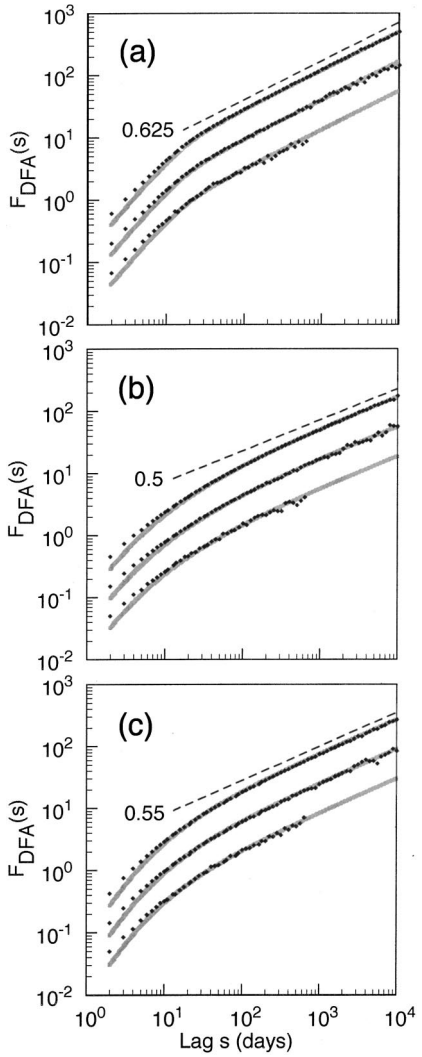

FIG. 4. Detrended fluctuation measures for synthetic time series of different lengths N as functions of the scale parameter s. In panel (a) the power spectral density of the time series is given by the piecewise linear model (4.2) with $\omega_0=0.1\pi$, $\beta_1=0.25$, and $\beta_2=2$. In panel (b) the power spectral density is a stretched exponential (4.1) with parameters $\omega_0=0.1\pi$ and $\gamma=0.65$, and in panel (c) the power spectral density is a Weibull distribution (4.3) with $\omega_0=0.14\pi$ and $\nu=0.9$. Each panel shows the results for different lengths of the time series. The resulting curves are shifted relative to each other by constant factors. The curves refer to time series of a length of $N=2^{19}$, 2^{15}, 2^{11} from top to bottom. The gray lines show the asymptotic $N \to \infty$ results given by Eqs. (3.12), (3.14) for the respective power spectral densities. Note that there is an excellent agreement even for the largest possible values of s. The deviations for small s are due to the continuum approximation used in (3.14). Only for the piecewise linear model a linear scaling regime can be identified. This is visible even for the shortest time series. As a guide of the eye, the broken straight line indicates the expected scaling behavior in (a), while in (b) and (c) the broken straight lines represent the expected asymptotic behavior.

IV. APPLICATION TO CLIMATE DATA

Near-surface temperature at most locations on the Earth shows considerable variations consisting of a strong diurnal and of an annual cycle with amplitudes of up to several tens of degrees. In a long-term average over several decades, these cycles are very regular, whereas on a day-to-day basis large deviations from the mean behavior may occur. These short-term deviations from the mean temperature behavior are governed by the synoptic weather conditions, the type of airmass, and surface properties near the given location. As the relevant physical processes are well understood, numerical weather models can in general reliably predict these short-term deviations several days ahead. Much less is known about temperature fluctuations on time scales between a month and decades.

To improve the understanding of climate and weather on these time scales, in a first step the correlation structure of temperature data can be analyzed to detect possible long-range correlations. This can be done in a standard way by means of the power spectral density. A summary of the climate spectrum from time scales of one hour up to the age of the Earth is presented in [14]. For periods less than one month the spectral density decreases with increasing frequency. However, the resolution of the data does not allow us to determine the type of spectral decay. In Ref. [15] daily

mean temperatures of a 30-year period were analyzed and their spectrum found to follow a stretched exponential, or exponential power [16] distribution

$$S_{se}(\omega) = S_0 \exp[-(\omega/\omega_0)^{\gamma}] \tag{4.1}$$

with three parameters S_0, ω_0, and γ. The exponent was found to be $\gamma \approx 0.54$ [15].

In Ref. [17] the asymptotic behavior of the power spectrum of 11 years' daily temperatures is investigated. For this purpose averages over large numbers of stations were performed. For over 1000 continental stations the average power spectral density has been fitted by a power law $S(\omega) \sim \omega^{-\beta}$ with an exponent $\beta_1 = 0.37$ in the low frequency limit and an exponent $\beta_2 = 1.37$ describing the high frequency behavior. The crossover between the two regimes is near the frequency corresponding to one month. The average power spectral density of 100 maritime stations scales in the whole frequency regime with the exponent $\beta = 0.63$ [17].

A. Data

Long time series of instrumental daily temperature values from Central Europe were analyzed in [18] for possible long-term trends. The same homogenized data are used for the present analyses. Daily mean temperature (obtained as mean of three temperature readings at fixed times), daily minimum, and daily maximum temperatures were available from four low-altitude stations, Basel-Binningen, Zürich-SMA, Bern-Liebefeld, and Neuchâtel, and from three mountain stations, Sonnblick, Säntis, and Zugspitze, all three located at an altitude higher than 2500 m. Details of the station locations are given in Table I of [18]. Zugspitze data are available from 1901 through 1992, with 106 days missing from May 1945 on. These missing values were replaced by the mean annual cycle giving time series of a length of 33 603 days. Sonnblick data are available from 1887 through 1993, with missing data at a few isolated periods of at most five days length. These gaps were filled by linear interpolation resulting in time series of 39 050 days. For the Swiss stations data from 1901 through 1997 are used, giving time series with a length of 35 429 days without any gaps.

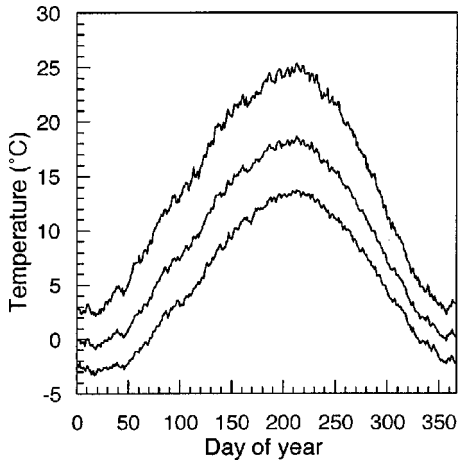

FIG. 5. Annual cycles of the maximum, mean, and minimum daily temperatures for Zürich.

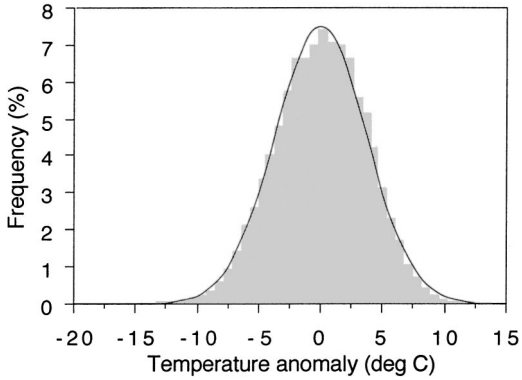

FIG. 6. Histogram of the anomalies of the mean daily temperatures for Zürich. The full line shows the Gaussian distribution with the mean value and variance estimated from the data.

Diurnal temperature data from the midlatitudes have a pronounced annual cycle. Thus, the power spectrum of the raw data has a strong peak at a frequency corresponding to one year. This annual peak will shadow many of the features of nearby frequency bands and obscure a possible scaling behavior. Therefore, the annual cycle is removed by subtracting the mean annual cycle from the data. This mean annual cycle is determined by calculating for each day of the year the average over all years of the time series, see Fig. 5. After removal of the mean annual cycle, time series of temperature

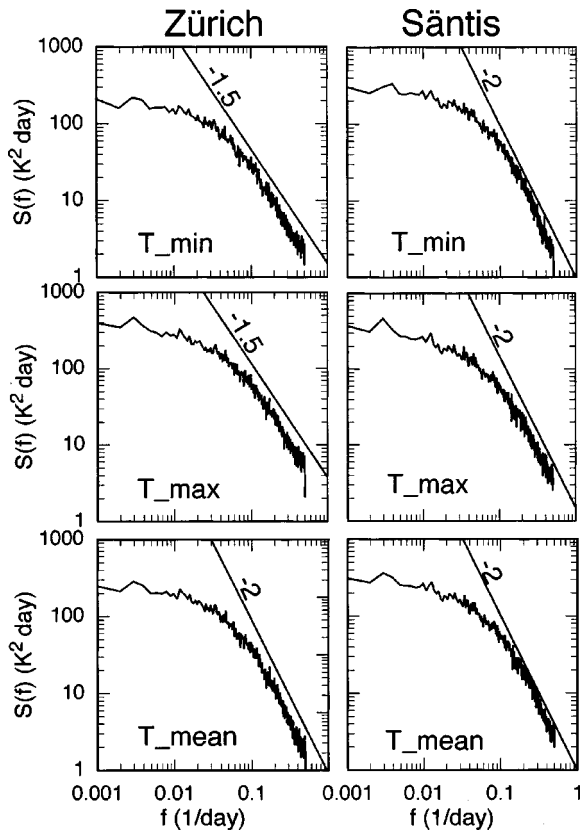

FIG. 7. Power spectral densities for different temperature series from Zürich and Säntis. The high frequency behavior is well described by a power law. A straight line with indicated slope is given to help the eye. At low frequencies a scaling assumption apparently describes the data less good.

anomalies are obtained, which will be used in the further analyses. Figure 6 shows a histogram of the Zürich mean temperature anomalies, which is quite well described by a Gaussian distribution with a standard deviation of 3.7 °C. The other temperature series give similar anomaly histograms with standard deviations ranging from 3.2 to 4.7 °C.

B. Power spectrum of daily temperatures

The power spectral densities of the temperature anomalies are calculated as described in Sec. II. The power spectral densities for frequencies higher than $2\pi/100$ are obtained as the averaged periodigrams of 68 blocks each of length 1024 d. For lower frequencies the average is performed over 16 blocks of length 4096 d. The power spectra of the two stations, Zürich and Säntis, representing low altitude and mountain stations, respectively, are shown in Fig. 7. The spectra of minimum, maximum, and mean temperatures of Säntis decay at large frequencies as ω^{-2} as well as those of the other mountain stations. The same high frequency dependence is also found for the mean values of the other Swiss low-altitude stations and stations in Hungary [19]. This corresponds to a random-walk-like behavior of the temperature on short time scales and in continuous time would correspond to a decay of the autocovariance with a finite slope at $t=0$. Minimum and maximum temperatures at Zürich and the other Swiss low altitude stations also approach the highest frequency in good approximation with a power low, however, as $\omega^{-1.5}$. The corresponding behavior of the correlation function in continuous time is a cusp with a square-root-like singularity at $t=0$. In discrete time these types of behavior cannot always be distinguished.

C. FA and DFA of daily temperatures

The variabilities $F_{FA}(s)$ of the daily temperatures are calculated by means of Eq. (2.5) for Zürich and Säntis and shown in Fig. 8. There are only minor differences between Zürich and Säntis and between maximum, minimum, and mean temperatures. The differences are more pronounced for larger lags s for both stations and are larger for Zürich than Säntis. In all cases the maximum temperatures show the largest variability, minimum and mean temperature variabilities are alway very close to each other. A clear scaling behavior is hard to identify in any of the displayed curves. The corresponding curves for the variability $F_{DFA}(s)$ of the detrended fluctuation analysis as given by Eq. (2.7), show even smaller deviations between the three types of temperatures. Therefore we show in Fig. 9 results only for the maximum Säntis temperature.

D. Comparison

For a better comparison we consider three different models that we formulate in terms of the power spectral density. The first one is a piecewise power law model, which reads

$$S_{pl}(\omega)=S_0\begin{cases}\left(\dfrac{\omega}{\omega_0}\right)^{-\beta_1} & \text{for } \omega<\omega_0\\ \left(\dfrac{\omega}{\omega_0}\right)^{-\beta_2} & \text{for } \omega_0\geqslant\omega.\end{cases} \tag{4.2}$$

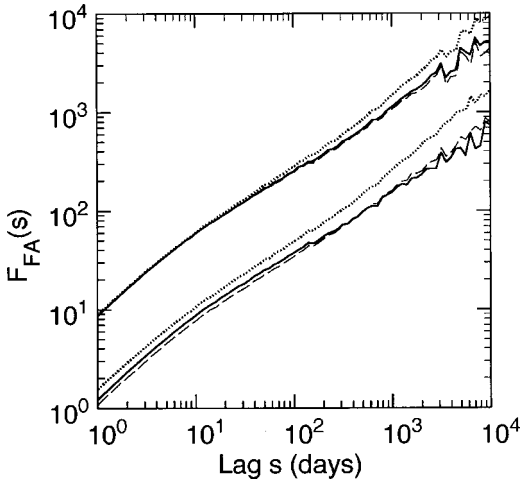

FIG. 8. Variability $F_{FA}(s)$ for daily temperatures from Zürich (upper group of curves) and Säntis (lower group of curves) as a function of the time lag s. The dotted lines correspond to maximum temperatures, the broken line to minimum and the solid line to mean temperatures. All curves relating to Säntis are multiplied by a factor of 8 such that they are separated from the respective curves of Zürich

The parameters chosen for the different stations and temperature series are collected in Table I. A similar model has been suggested in Ref. [17] with $\beta_1=0.37$ and $\beta_2=1.37$ being in rough agreement with our findings for low-altitude stations. In Ref. [20] a three-year record of 3-h ambient temperatures was analyzed. The high frequency exponent 1.78 is close to ours, whereas the low frequency exponent $\beta_1=0.72$ is considerably larger than what we find; see Table I. The discrepancy may partly be caused by the shorter time series used in [20] but also by the fact that the annual cycle was not removed from the data.

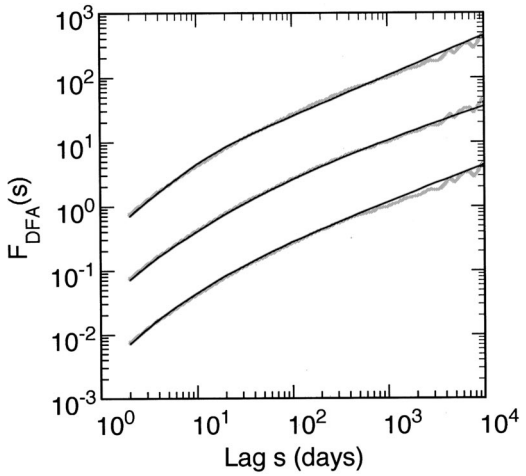

FIG. 9. The three black curves represent the variabilities $F_{DFA}(s)$ resulting from the piecewise power law (upper curve), the stretched exponential (middle curve), and the Weibull (lowest curve) power spectral densities with parameters obtained from maximum temperatures of Säntis, see also Fig. 10 below. The upper and lower curves are multiplied by factors of 10 and 10^{-1}, respectively for better visibility. The gray curves show the results of DFA for the maximum temperatures of Säntis.

TABLE I. Parameters of the power law model (4.2) for the spectral density for the stations Sonnblick (SO), Säntis (SA), Zugspitze (ZU), Basel-Binningen (BA), Zürich SMA (ZH), Bern-Liebefeld (BE), and Neuchâtel (NE). The parameter β_2 equals 2 except for the minimum and maximum temperature at the stations BA, ZH, BE, and NE, where $\beta_2 = 1.5$.

	Minimum temperature			Maximum temperature			Mean temperature		
	S_0	ω_0	β_1	S_0	ω_0	β_1	S_0	ω_0	β_1
SO	147	0.34	0.19	133	0.31	0.20	136	0.33	0.20
SA	147	0.33	0.22	129	0.39	0.28	139	0.35	0.23
ZU	135	0.36	0.22	129	0.37	0.23	127	0.37	0.22
BA	115	0.23	0.25	177	0.25	0.26	122	0.28	0.24
ZH	105	0.22	0.22	164	0.29	0.28	119	0.29	0.24
BE	86	0.27	0.31	163	0.26	0.23	107	0.29	0.25
NE	72	0.27	0.35	141	0.25	0.28	97	0.29	0.28

The second model is defined by a stretched exponential power spectral density as given in Eq. (4.1). The parameter values that fit the data best are given in Table II. Finally, we compare with a power spectral density that is given by a Weibull distribution:

$$S_{We} = S_0(\omega/\omega_0)^{\nu-1} \exp[-(\omega/\omega_0)^{\nu}]. \tag{4.3}$$

The parameters S_0, ω_0, and ν of this model are given in Table III. A comparison of these models with the power spectral density for the Säntis maximum temperatures is shown in Fig. 10. All three models fit the data reasonably well. The discontinuity of the slope at the merging point of the different power laws in $S_{pl}(\omega)$ and a too steep decay of $S_{We}(\omega)$ at high frequencies present the main visible deviations of the model spectra from the data. The stretched exponential model qualitatively differs from the other two models in that it approaches a constant value of the power spectral density at zero frequency, while the other two models diverge there. However, the comparison of the spectral densities does not reveal this difference because of the finite amount of observations.

For all three models, the autocovariances decay according to an algebraic law, $t^{-\alpha}$. For the piecewise power law model the exponent is $\alpha = 1 - \beta_2$, and for the Weibull model $\alpha = \nu$. In the present cases the resulting exponents α are positive and smaller than one and roughly coincide with each other. Most of them are larger than the value of $\alpha = 2/3$ given in [4]. The stretched exponential model with a positive exponent $\gamma < 1$ leads to the autocovariance exponent $\alpha = 1 + \gamma$ and, hence, is even larger than one. Again, from the data these different types of behavior cannot be distinguished because of their finite lengths, see Fig. 11. In Table IV the values of the exponents α for different stations and different temperature types are compared as they result from fits of the three model power spectral densities and from the data by means of DFA.

TABLE II. Parameters of the stretched exponential model (4.1) for the spectral density for the same stations as in Table I.

	Minimum temperature			Maximum temperature			Mean temperature		
	S_0	ω_0	γ	S_0	ω_0	γ	S_0	ω_0	γ
SO	307	0.33	0.77	286	0.28	0.73	291	0.30	0.73
SA	331	0.29	0.74	442	0.18	0.57	354	0.25	0.67
ZU	320	0.29	0.71	325	0.27	0.67	307	0.28	0.69
BA	306	0.16	0.59	515	0.15	0.56	310	0.20	0.68
ZH	245	0.20	0.65	527	0.15	0.53	294	0.22	0.69
BE	336	0.10	0.48	409	0.20	0.61	291	0.19	0.61
NE	372	0.06	0.41	487	0.11	0.51	302	0.15	0.59

TABLE III. Parameters of the Weibull model (4.3) for the spectral density for the same stations as in Table I.

	Minimum temperature			Maximum temperature			Mean temperature		
	S_0	ω_0	ν	S_0	ω_0	ν	S_0	ω_0	ν
SO	232	0.46	0.93	205	0.43	0.93	209	0.46	0.93
SA	237	0.44	0.92	215	0.48	0.85	223	0.46	0.90
ZU	220	0.47	0.92	207	0.48	0.90	204	0.48	0.91
BA	155	0.41	0.85	247	0.43	0.85	200	0.36	0.90
ZH	146	0.39	0.88	228	0.49	0.83	193	0.38	0.90
BE	117	0.46	0.80	227	0.44	0.88	174	0.38	0.88
NE	97	0.48	0.76	195	0.43	0.82	158	0.37	0.86

Finally, within the time scales of lags for which the DFA variability can be reliably estimated, only the piecewise power law model shows a well defined scaling behavior for large lags s. Both the stretched exponential and the Weibull model show a slight curvature up to the largest observable lags. The comparison with the data is shown in Fig. 9. It is equally good for all three models of which the stretched exponential shows the most pronounced, but still rather small, deviations for large lags.

V. SUMMARY

We have investigated the question of whether FA or DFA do provide insight in the long time behavior that goes be-

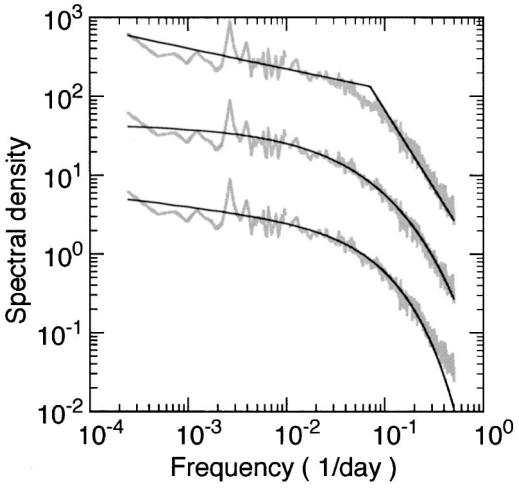

FIG. 10. Piecewise power law, stretched exponential, and Weibull power spectral densities (black lines), from top to bottom, compared to the estimated spectra for the Säntis maximum temperatures (gray lines). Spectra are stretched relative to each other by factors of 10 for better visibility.

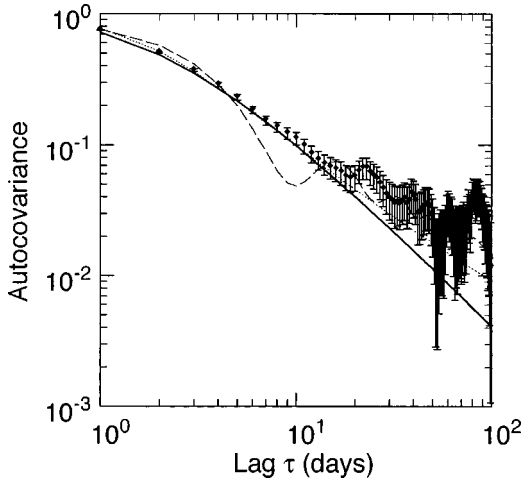

FIG. 11. Autocovariances resulting from the piecewise power law (broken line), stretched exponential (solid line), and Weibull (dotted line) power spectral densities, each with the parameters of the Säntis maximum temperatures as shown in Fig. 10 compared with the autocovariance directly estimated from the data (points). The error bars are estimated according to Ref. [22] and indicate the statistical uncertainty. For time lags larger than 100 the error bars become larger than the estimated values of the autocovariance.

yond the possibilities of spectral analysis. An important advantage of FA and DFA lies in the fact that, for a stationary process, the variability measures $F^2_{FA}(s)$ and $F^2_{DFA}(s)$ are self-averaging, i.e. the estimate of the variability measures from finite time series, as given by Eq. (2.5) in case of FA, converge in the limit of infinite time series towards the ensemble average of $F^2_{FA}(s)$. One can show that for a process with decaying autocovariance the variance of the squared variability measure (2.5) determined from a finite time series of length N converges to zero as $N^{-1/2}$. The same also holds for DFA. Therefore no extra averaging procedures are necessary for FA and DFA as they have to be performed in spectral analysis. This renders FA and DFA a more systematic procedure in contrast to spectral analysis, which is something of an art. However, one must not forget that for time series of finite lengths the variability at large lags s may still have large statistical uncertainties. We have illustrated these finite size effects with a few examples of synthetic time series with prescribed power spectral densities. In all cases we find surprisingly small finite size effects. This is certainly a strong virtue of the detrended fluctuation analysis. We also investigated the finite size effects for fluctuation analysis with very similar results as for the DFA.

For stationary time series, which do not decay according to a power law, FA and DFA do not seem to represent particularly convenient instruments to identify or distinguish concrete models.

For the ambient temperature time series of the 20th century it is not possible to distinguish by means of DFA between models that are compatible with the observed power spectral densities. Yet the different models lead to significantly different scaling behavior of the autocovariance decay. Though it is not possible to identify a definite optimal model by means of FA or DFA, these methods unambiguously show long time correlations of the temperature fluctuations that extend up to the longest observable time lags. Without these correlations the FA and DFA fluctuation measures would scale with the exponent 0.5 at large lags. Our analysis has shown that one third of the total length of the time series represents a conservative estimate for the largest observable lag. Hence, the temperature fluctuations are correlated up to at least 30 years. These long time effects are most likely caused by the ocean dynamics, which interacts with that of the atmosphere.

The FA variability measure $F^2_{FA}(s)$ coincides with the structure function as defined in the theory of turbulence [21], if one interprets the integrated process $y(t)$ as the velocity of a turbulent field measured at a fixed point in space. So far, only the second-order structure function has been used in FA. If $F_{FA}(s)$ shows scaling at large lags s it would be interesting to also ask about the behavior of the higher order structure functions $F^p_{FA}(s)=\langle|\Delta y_{s_0}(s)|^p\rangle$. For an underlying Gaussian process a trivial scaling will result, i.e., $F^p_{FA}(s) \sim [F^2_{FA}(s)]^{p/2} \sim s^{p\zeta_2/2}$, whereas non-Gaussian processes will give rise to intermittency corrections, i.e., $F^p_{FA} \sim s^{\zeta_p}$, where $\zeta_p \neq p\zeta_2/2$. Since we could not identify an unambiguous scaling regime in the temperature time series we did not pursue this direction further.

We have always assumed that the underlying process $x(t)$ is stationary or, at most has a linear trend that is automatically removed by DFA. If this is not the case, one can still calculate variability measures of finite time series. They will explicitly depend on the initial instant of time t_0 at which the series begins and on the length N of the series. In general one

TABLE IV. Scaling exponents of the autocovariance decay $t^{-\alpha}$ for the power law (PL) spectrum, the stretched exponential (SE) spectrum, the Weibull (WE) spectrum, and as obtained by DFA. Data from the same stations as in Table I are used.

	Minimum temperature				Maximum temperature				Mean temperature			
	PL	SE	WE	DFA	PL	SE	WE	DFA	PL	SE	WE	DFA
SO	0.81	1.77	0.93	0.74	0.80	1.73	0.93	0.72	0.80	1.73	0.93	0.68
SA	0.78	1.74	0.92	0.72	0.72	1.57	0.85	0.64	0.77	1.67	0.90	0.66
ZU	0.78	1.71	0.92	0.68	0.77	1.67	0.90	0.68	0.78	1.69	0.91	0.68
BA	0.75	1.59	0.85	0.68	0.74	1.56	0.85	0.62	0.76	1.68	0.90	0.72
ZH	0.78	1.65	0.88	0.74	0.72	1.53	0.83	0.66	0.76	1.69	0.90	0.72
BE	0.69	1.48	0.80	0.70	0.77	1.61	0.88	0.66	0.75	1.61	0.88	0.66
NE	0.65	1.41	0.76	0.66	0.72	1.51	0.82	0.66	0.72	1.59	0.86	0.64

cannot expect a convergence of the variabilities as a function of N, i.e., one cannot expect self-averaging. But even if the variability measures converged in the limit $N\to\infty$ the resulting functions represent averages over different inequivalent parts of the time series. The resulting average behavior of the variability may be atypical when compared with the true variability of the time series taken during any particular time interval.

ACKNOWLEDGMENTS

Valuable comments by Dr. Remo Badii are gratefully acknowledged. We thank the Schweizerische Meteorologische Anstalt, the Deutscher Wetterdienst, and the Zentralanstalt für Meteorologie und Geophysik for kindly providing the data used in this study.

APPENDIX: THE DISCRETE CASE

In the case of a discretely sampled time series $x_n = x(n\Delta t)$ one finds from Eq. (2.5) for the variability measure of fluctuation analysis the expression

$$F_{FA}^2(l\Delta t) = \sum_{u=-l}^{l} (l-|u|)C(u\Delta t)(\Delta t)^2. \tag{A1}$$

The autocovariance $C(u\Delta t)=\langle x_{k+u}x_k\rangle$ of the stationary, discrete process, x_k, can be expressed in terms of the power spectral density $S(\omega)$

$$C(u\Delta t) = \frac{1}{2\pi}\int_0^\pi d\omega \cos(\omega u\Delta t)S(\omega). \tag{A2}$$

Consequently one finds for the variability

$$F_{FA}^2(l\Delta t) = \frac{1}{2\pi}\int_0^\pi d\omega r_l^{FA}(\omega)S(\omega), \tag{A3}$$

where

$$r_l^{FA}(\omega) = \sum_{u=-l}^{l} (l-|u|)\cos(\omega u\Delta t)(\Delta t)^2 = \frac{1-\cos(\omega s\Delta t)}{1-\cos(\omega\Delta t)}(\Delta t)^2. \tag{A4}$$

For large values of l and small frequencies ω the filter $r_l^{FA}(\omega)$ approaches the continuum limit, see Eq. (3.4).

For a discretely sampled time series the expression (2.7) of the detrended fluctuation analysis yields after some algebra:

$$F_{DFA}^2(l\Delta t) = \frac{1}{1+l}\sum_{u=0}^{l} q_l(u)C(u\Delta t)\Delta t, \tag{A5}$$

where the filter function $q_l(u)$ is defined by

$$q_l(u) = \frac{l^2+2l-3}{15}\delta_{u,0}\Delta t + (1-\delta_{u,0}) \times\left(\frac{1}{5l(l+1)(l+2)}u^5 - \frac{4l^2+8l+3}{3l(l+1)(l+2)}u^3 + 2u^2 - \frac{15l^4+60l^3+55l^2-10l-12}{15l(l+1)(l+2)}u + \frac{2(l^2+2l-3)}{15}\right)\Delta t. \tag{A6}$$

As a function of u the filter has its maximum at $u=0$, becomes zero at approximately $u=0.2l$, shows a minimum near $u=0.4l$, and again is zero at $u=l$. Expressing the autocovariance by the spectral density one finds for the variability

$$F_{DFA}^2(l\Delta t) = \frac{1}{2\pi}\int_0^\pi d\omega r_l^{DFA}(\omega)S(\omega), \tag{A7}$$

where

$$r_l^{DFA}(\omega) = \frac{1}{l+1}\sum_{u=0}^{l}\cos(\omega u\Delta t)q_l(u). \tag{A8}$$

The explicit expression of the filter $r_l^{FD}(\omega)$ is rather involved and will not be given here. As a function of ω, $r_l^{FD}(\omega)$ is zero at $\omega=0$, increases quadratically and reaches a maximum that moves closer towards $\omega=0$ with increasing l, and, at the same time increases. Between the maximum and $\omega\Delta t=\pi$ one observes a monotonic decrease of $r_l^{FD}(\omega)$. At $\omega\Delta t=\pi$ the frequency filter $r_l^{FD}(\pi)$ apparently approaches 1/4 from below in the limit $l\to\infty$.

In the limit of large l the filter function $q_l(u)$ scales according to $q_l(u)=l^2q(u/l)+O(l^{-1})$, where $q(u)$ is given by (3.11) and the sum can be approximated by an integral with the final result of the continuum limit as given in Eq. (3.10).

[1] C.-K. Peng, S. V. Buldyrev, A. L. Goldberger, S. Havlin, F. Sciortino, M. Simons, and H. E. Stanley, Nature (London) **356**, 168 (1992).

[2] C.-K. Peng, S. V. Buldyrev, A. L. Goldberger, S. Havlin, M. Simons, and H. E. Stanley, Phys. Rev. E **47**, 3730 (1993).

[3] C.-K. Peng, S. V. Buldyrev, S. Havlin, M. Simons, H. E. Stanley, and A. L. Goldberger, Phys. Rev. E **49**, 1685 (1994).

[4] E. Koscielny-Bunde, H. E. Roman, A. Bunde, S. Havlin, and H.-J. Schellnhuber, Philos. Mag. B **77**, 1331 (1998).

[5] S. V. Buldyrev, A. L. Goldberger, S. Havlin, R. N. Mantegna, M. E. Matsa, C.-K. Peng, M. Simons, and H. E. Stanley, Phys. Rev. E **51**, 5084 (1995).

[6] C. P. Peng, S. Havlin, J. M. Hausdorff, J. Mietus, H. E. Stanley, and A. L. Goldberger, J. Electrocardiol. **28**, 59 (1996).

[7] R. A. Absil, R. Sepulchre, A. Bilge, and P. Gérard, Physica A **272**, 235 (1999).

[8] N. Vandewalle and M. Ausloos, Physica A **246**, 454 (1997).

[9] E. Koscielny-Bunde, A. Bunde, S. Havlin, and Y. Goldreich, Physica A **231**, 393 (1996).

[10] E. Koscielny-Bunde, A. Bunde, S. Havlin, H. E. Roman, Y.

Goldreich, and H.-J. Schellnhuber, Phys. Rev. Lett. **81**, 729 (1998).
[11] A. A. Tsonis, P. J. Roebber, and J. B. Elsner, Geophys. Res. Lett. **25**, 2821 (1998).
[12] A. A. Tsonis, P. J. Roebber, and J. B. Elsner, J. Clim. **12**, 1534 (1999).
[13] W. H. Press, S. A. Teukolsky, W. T. Vetterling, and B. P. Flannery, *Numerical Recipes in Fortran. The Art of Scientific Computing*, 2nd ed. (Cambridge University Press, Cambridge, 1992).
[14] J. M. Mitchell, Jr., Quaternary Research **6**, 481 (1976).
[15] I. M. Jánosi and G. Vattay, Phys. Rev. A **46**, 6386 (1992).
[16] E. B. Manoukian, *Modern Concepts and Theorems of Mathematical Statistics* (Springer-Verlag, New York, 1986).
[17] J. D. Pelletier, J. Clim. **10**, 1331 (1997).
[18] R. O. Weber, P. Talkner, and G. Stefanicki, Geophys. Res. Lett. **21**, 673 (1994).
[19] I. M. Jánosi, G. Vattay, and A. Harnos, J. Stat. Phys. **93**, 919 (1998).
[20] Ph. Ladoy, S. Lovejoy, D. Schertzer, in *Non-Linear Variability in Geophysics*, edited by D. Schertzer and S. Lovejoy (Kluwer, Dordrecht, 1991), p. 241.
[21] A. S. Monin, and A. M. Yaglom, *Statistical Fluid Mechanics: Mechanics of Turbulence* (MIT Press, Cambridge, MA, 1975), Vol. 2.
[22] M. S. Bartlett, Suppl. J. Roy. Stat. Soc. **8**, 27 (1946).